Available online at www.sciencedirect.com
SCIENCE DIRECT®
Journal of Solid State Chemistry 177 (2004) 4404–4412
JOURNAL OF SOLID STATE CHEMISTRY
www.elsevier.com/locate/jssc

The pyrochlore to 'defect fluorite' transition in the $Y_2(Zr_yTi_{1-y})_2O_7$ system and its underlying crystal chemistry

Yun Liu, Ray Leslie Withers*, Lasse Norén

Research School of Chemistry, Solid State Structural Chemistry, Australian National University, Building 35, Science Road, Canberra, Australian Capital Terr 0200, Australia

Received 16 July 2004; received in revised form 1 September 2004; accepted 10 September 2004
Available online 11 November 2004

Abstract

A careful investigation of the previously reported single phase, pyrochlore structure type $Y_2(Zr_yTi_{1-y})_2O_7$, $0 \leqslant y \leqslant 0.9$, (YZT) solid solution has been carried out. Given the known slow rate of diffusion of cations in fluorite-related stabilized zirconia systems and the consequent difficulty in achieving equilibrium, careful attention was paid to synthesis procedures while Guinier XRD and electron diffraction were used to investigate the synthesized materials. As a consequence, a subtle but nonetheless clear two-phase region separating a pyrochlore-type solid solution field (from $0 \leqslant y \leqslant \sim 0.54$) from a "defect fluorite" type solid solution field (from $\sim 0.68 \leqslant y \leqslant 1$) has been found. The underlying crystal chemistry of the system has been investigated using the bond valence sum approach. The dielectric properties have also been measured as a function of composition. The dielectric constant and dielectric loss of the lowest y compounds are potentially quite useful but deteriorate rapidly with increasing Zr content.

Keywords: Pyrochlore to "defect fluorite" phase transition; $Y_2(Zr_yTi_{1-y})_2O_7$ system; Bond valence sum study; Electron diffraction investigation

1. Introduction

"Defect fluorite"-type yttrium-stabilized zirconia is currently widely used as the solid electrolyte of choice in solid oxide fuel cells (SOFCs) as well as in sensors measuring oxygen partial pressure in car exhaust systems, as a result of its high oxide ion conductivity at moderate to high temperature as well as its low activation energy for such oxide ion conduction [1]. Such properties, however, are not the only desirable characteristics required for use in SOFCs. Another very important physical requirement is chemical stability and compatibility with adjoining electrode materials [2]. There has therefore been much recent interest in a monolithic fuel cell design in which cathode, electrolyte and anode are inherently compatible as a result of being made up of essentially the same $A_2(B_y'B_{1-y})_2O_7$ ($A = Y^{3+}, Gd^{3+}$; $B = Ti^{4+}$; $B' = Zr^{4+}, Sn^{4+}$) 'pyrochlore'-type (mixed oxide ion as well as electronically conducting) materials [2–6]. (Note that the ideal $A_2B_2O_7$ pyrochlore structure type [see Fig. 1] can be described as a cation and oxygen vacancy ordered $2 \times 2 \times 2$ superstructure of an underlying 'defect fluorite'-type parent structure, see e.g., [7,8].)

Particular interest has focussed on the $Y_2(Zr_yTi_{1-y})_2O_7$ system as a result of the electronic conductivity introduced by the presence of the Ti ions as well as the "...remarkable increase in (oxide ion) conductivity of three orders of magnitude as the Ti cation is replaced by the larger Zr cation..." [5]. Further (intense) interest in this particular system has been generated by the rather detailed insight into the mechanism of disorder involved in the pyrochlore to "defect fluorite" transition as a function of increasing y in this system obtained by neutron powder diffraction investigation [2,9], largely as a result of the extraordinary sensitivity of the latter to the so-called 'pyrochlore-type' $\mathbf{G} \pm \frac{1}{2}\langle 111 \rangle^*$ (**G** an

*Corresponding author. Fax: +61 2 6125 0750.
E-mail address: withers@rsc.anu.edu.au (R.L. Withers).

0022-4596/$ - see front matter © 2004 Elsevier Inc. All rights reserved.
doi:10.1016/j.jssc.2004.09.014

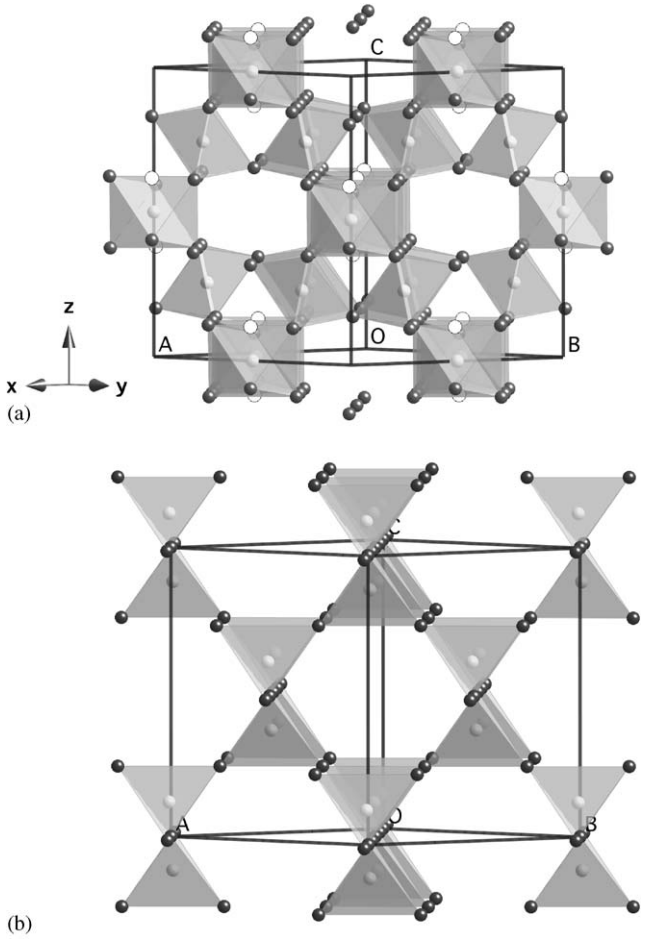

Fig. 1. The two interpenetrating network structure types that together constitute the ideal pyrochlore structure type in projection close to a ⟨110⟩ orientation. The first network (see Fig. 1(a)) is a $((Ti_{1-y}Zr_y)^{4+})_2O(1)_6$ array of corner-connected, cation-centered 'octahedra' (the initially unoccupied O(3) sites are represented by the small white balls while the initially fully occupied O(1) sites are represented by the small dark balls). The second network (see Fig. 1(b)) is an $O(2)(Y^{3+})_2$ array of corner-connected, oxygen-centered tetrahedra (of 'ideal' anti-β-cristobalite structure type).

allowed parent fluorite-type Bragg reflection) satellite reflections.

Thus, Heremans et al. [2,9] were able to show that structural disorder in this system involved substitution of dopant Zr ions for Ti ions on the 'octahedral' pyrochlore *B* (or 16*d*) sites coupled with a simultaneous gradual filling of the initially unoccupied *O*3 (or 8*b*) sites at the expense of the initially fully occupied *O*1 (or 48*f*) sites (see Fig. 1a) until $y\sim0.50$–0.55, at which stage cation disorder on the pyrochlore A (or 16*c*) site and depletion of the *O*2 (or 8*a*) site was reported to set in (see Fig. 1b) [2,9]. Complete mixing of all three cation species was only then reported to occur "... abruptly over the composition range $0.60<y\leqslant0.90$.." [9]. The refined behavior as a function of composition of the one unknown fractional co-ordinate of the pyrochlore structure type, the x fractional co-ordinate of the *O*1 ion, $x=\frac{3}{8}+\varepsilon$, was furthermore used to propose a continuous pyrochlore-type solid solution for $0\leqslant y\leqslant\sim0.9$, at which stage a transition to complete structural disorder, i.e., to a "defect fluorite", was reported to occur [2,9]. These results have subsequently inspired a diverse range of spectroscopic investigations of disorder and local co-ordination environments in this and closely related systems (see e.g., [10–12]).

Of course, the interpretation as well as the validity of such results depends upon the implicit assumption of the neutron diffraction study that the underlying, long range ordered, average structure is genuinely of pyrochlore structure type right across the reported $Y_2(Ti_{1-y}Zr_y)_2O_7$, $0\leqslant y\leqslant\sim0.90$, solid solution field. That this should be so, however, is not so obvious, particularly at the higher y, higher ionic conductivity end [5] of this proposed solid solution where the reported results contradict published phase analysis studies [13,14] which report that the "defect fluorite" solid solution field is by no means limited to the range from $y=1$ to ~0.9 but rather extends all the way from $y=1$ to ~0.6. (Note that the detection of intensity at the $G\pm\frac{1}{2}\langle111\rangle^*$ regions of reciprocal space is not necessarily an infallible indicator of the presence of a pyrochlore rather than "defect fluorite" phase—see e.g., [8,15–18].)

Likewise, some of the spectroscopic results on this YZT system [10–12] also raise the possibility of a pyrochlore to "defect fluorite" transition well before $y=0.9$ e.g., the marked similarity of the ^{17}O MAS NMR spectra of the end-member $y=1$ compound (known to be in the "defect fluorite" phase) and the $y=0.8$ compound suggest that the latter is also in the "defect fluorite" phase, while the marked contrast of both spectra with that of the $y=0.3$ compound [11] suggests that the phase transition from pyrochlore to "defect fluorite" takes places somewhere between $y=0.3$ and 0.8. Unfortunately, the reported neutron diffraction study [2,9] investigated only $y=0.3$, 0.45, 0.60, and 0.90 specimens leaving a large gap in the controversial region between 0.6 and 0.9 [13,14].

It is noted that Heremans et al. [2,9] reported evidence for a minority fluorite-like phase "... with a lattice constant slightly larger than $a/2$ of the pyrochlore superstructure phase ... in an amount that increased with y ..." [9] co-existing with a majority pyrochlore-type phase in all their specimens. A conventional two-phase miscibility gap interpretation, however, was ruled out on the grounds of the unusual observed lattice parameter behavior. Despite the emphasized minor presence of this fluorite-type phase [2,9], such behavior suggests problems in achieving complete equilibrium and has to raise at least some doubt as to the exact composition of the synthesized samples. Given the known extremely slow rate of diffusion of cations in

fluorite-related stabilized zirconia systems, this is perhaps not too surprising.

Given the importance of understanding the connection between structure (albeit inherently disordered) and function (mixed oxide ion and electronic conduction) in such systems, the primary purpose of the current paper is to use powder XRD in conjunction with electron diffraction (a technique well-suited to the detection of subtle structural changes) to carefully investigate the existence or otherwise of a pyrochlore to "defect fluorite" phase transition in the $Y_2(Zr_yTi_{1-y})_2O_7$ (YZT) system. A subsidiary aim is to use the bond valence sum method to obtain an improved crystal chemical understanding of the observed crystallographic behavior.

2. Synthesis

Two synthesis routes were used to attempt to synthesize the desired single phase $Y_2(Zr_yTi_{1-y})_2O_7$ (YZT) compounds, the first a conventional solid-state synthesis approach and the second a metallo-organic decomposition (MOD) process. Initially, solid-state reaction was used. High purity Y_2O_3, ZrO_2 and TiO_2 raw materials were thus mixed together in the correct proportions to form the compounds $Y_2(Zr_{0.5}Ti_{0.5})_2O_7$ and $Y_2(Zr_{0.7}Ti_{0.3})_2O_7$ and then ground homogeneously under ethanol in an agate mortar. The resultant mixture was then pressed into pellets (the typical size was 10 mm in diameter and ~1 mm in height) and calcined at 1350–1500 °C for a period of 20 days with intermediate grinding and re-pelleting. The resultant specimens, however, gave somewhat broad lines in Guinier XRD patterns and were always found to be two-phase (pyrochlore plus "defect fluorite") via electron diffraction (see below). The solid-state route was thus abandoned in favor of the following MOD process in an attempt to ensure greater homogeneity of the precursor starting materials and hence lower annealing temperatures as well as a greater likelihood of equilibrium resultant material.

In total, 3.8301 g of yttrium nitrate ($Y(NO_3)_3 \cdot 6H_2O$, Alfa, 3N) was completely dissolved into 30 ml of ethylene glycol monomethyl ether (EGME, $C_3H_8O_2$) solvent by stirring. The appropriate stoichiometric ratios of titanium isopropoxide ($Ti(OCH(CH_3)_2)_4$, 97%, Aldrich) and zirconium propoxide ($Zr(OCH_2CH_2CH_3)_4$, 70 wt%, Aldrich) were then added and stirred whilst gently heating until the transparent and uniform solution transformed to a gel. This gel was then thermally treated, firstly at 200 °C to remove the solvent, secondly at 600 °C for 30 min for combustion and decomposition of the NO_3^- groups, and finally at 850 °C for 15 h to eliminate CO_2 through heat treatment. The resultant powders were then pressed into pellets and calcined at 1350 °C for periods between 5 and 20 days with intermediate grinding and re-pelleting. YZT compounds with compositions $y = 0.1$, 0.2, 0.3, 0.4, 0.5, 0.6, 0.7 and 0.8 were thereby readily synthesized.

3. Experimental

The phase purity of these samples was carefully investigated via X-ray powder diffraction using a Guinier–Hägg XRD camera with Cu$K\alpha$1 radiation. Silicon (NBS No. 640C) was added as an internal standard for accurate determination of the unit cell dimensions, which were refined using the Unitcell software package [19]. Transmission electron microscope (TEM) investigation was carried out in a Philips EM 430 TEM on crushed grains of the samples dispersed onto holey carbon-coated copper grids.

For the dielectric measurements, silver paste (Dupont) was brushed onto the two surfaces of previously polished pellets (typical size 10 mm in diameter and ~1 mm in height), which were then subjected to thermal treatment at 500 °C for 30 min for solidification and to ensure good electrical contact as electrodes. Pt wire was then affixed upon the two electrodes for high temperature measurement. The dielectric properties (dielectric constant and dielectric loss) were then measured using a high precision LCR meter (Agilent 4284A).

4. Results

4.1. XRD

The $y = 0.5$ and 0.7 solid-state synthesized samples were always found to be two-phase (consisting of an ordered pyrochlore and a disordered "defect fluorite") even after annealing at 1500 °C for 20 days. On the other hand, single phase samples giving rise to noticeably sharper lines in Guinier XRD films were routinely and reproducibly achievable using the MOD process followed by annealing at considerably lower temperatures (1350 °C) for considerably shorter periods of time (~5 days).

In the MOD process, oxolation (a condensation reaction in which an *oxo bridge* (-O-) is formed between metal centers [20]) occurs rapidly in solution with little energy cost. The homogeneity at the molecular level coupled with the prior formation of a metal-oxygen-metal network in the precursor solution leads to a much lower activation energy for crystallization and is consistent with the fact that a single phase YZT sample could be readily achieved over virtually the whole composition range after annealing at only 1350 °C for 5 days.

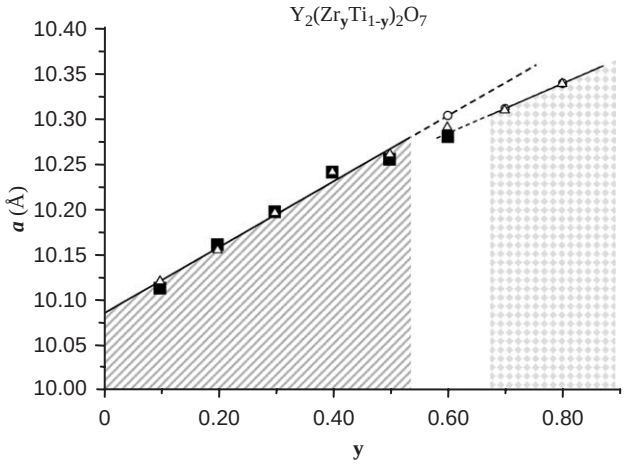

Fig. 2. A plot of twice the refined cubic fluorite, parent unit cell dimension (corresponding to the pyrochlore unit cell dimension) of the MOD synthesized samples as a function of Zr content, y, in the $Y_2(Zr_yTi_{1-y})_2O_7$ system. The open triangles correspond to 5 h annealed, single-phase specimens. The filled squares and the open circles correspond to 20 h annealed specimens, of pyrochlore and defect fluorite type, respectively. The $y = 0.60$ specimen is two phase for the 20 h annealed specimen.

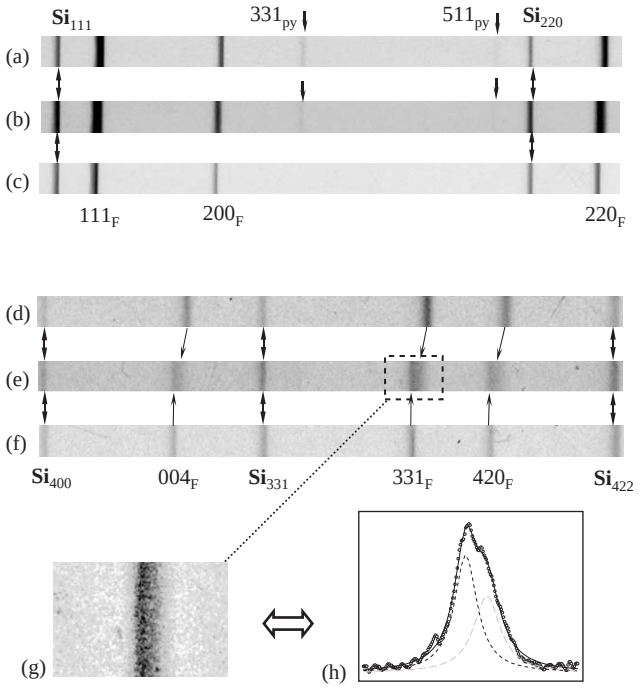

Fig. 3. Scanned Guinier XRD films of the $y = 0.5$, 0.6 and 0.7 compounds at both low angle (*a*, *b* and *c*) and high angle (*d*, *e* and *f*), respectively. Fig. 3g shows a blowup of the very broad ('split') $\langle 331 \rangle_F^*$ line (see the dashed box in Fig. 3e) for the $y = 0.6$ sample while Fig. 3h shows a scanned trace of the same reflection along with a Lorentzian fit requiring the use of two quite distinct lines.

By contrast, the solid-state reaction process requires the very stable metal-oxygen bonding in the raw oxide materials to first of all be broken prior to re-crystallization and clearly requires a rather larger activation energy. Likewise, the diffusion coefficients for the metal ions in these solid oxides is many orders of magnitude smaller than is the case in the MOD process, thus homogeneity is much more difficult to obtain in the solid-state reaction process. This suggests that the 1350–1500 °C annealing temperatures available to us were insufficient to produce equilibrium single-phase YZT samples in the case of the solid-state synthesis. The MOD synthesized samples were thus taken as genuinely equilibrium samples whereas the solid-state synthesized materials were not.

Fig. 2 shows a plot of twice the refined cubic fluorite, parent unit cell dimension (corresponding to the pyrochlore unit cell dimension) of these MOD synthesized samples as a function of Zr content, y, in the $Y_2(Zr_yTi_{1-y})_2O_7$ system. The refined lattice parameters are in remarkably good agreement with those reported by Heremans et al. [9] (cf. Fig. 2 with, for example, Fig. 4 of [9]), except for the existence of the two-phase region centered around $y = 0.6$ (see below). The estimated width of the two-phase region (based on the refined lattice parameters of the end-member phases in the $y = 0.6$ sample) is $\sim 0.54 \leqslant y \leqslant \sim 0.68$ (see Fig. 2). As also reported by Heremans et al. [9], the lattice parameter was found to increase essentially linearly with Zr content in apparent agreement with Vegard's law.

For similar exposure times, the widths of the various lines in the Guinier films visually behaved very similarly as a function of composition except for the $y = 0.6$ sample which invariably showed broadened peaks relative to other compositions particularly at high angle, suggesting the possibility of a two-phase region. After longer annealing (another 15 days at 1350 °C), the additional asymmetric broadening ('splitting') of the high angle peaks for this $y = 0.6$ composition became quite noticeable in the Guinier film (cf. Fig. 3e with Figs. 3d and f; see also Fig. 2). This did not happen with the other single-phase compounds. Fig. 3 shows scanned Guinier XRD films of the $y = 0.5$, 0.6 and 0.7 compounds at both low angle (Figs. 3a, b and c) and high angle (Figs. 3d, e and f) respectively. Fig. 3g shows a blow up of the very broad ('split') $\langle 331 \rangle_F^*$ line (see the dashed box in Fig. 3e) for the $y = 0.6$ sample while Fig. 3h shows a scanned trace of the same reflection. Fig. 3h also shows a Lorentzian fit to the same reflection requiring the use of two quite distinct lines. In addition, note that the pyrochlore-type satellite reflections (labeled 331_{py} and 511_{py} in Figs. 3a and b) while present in the $y = 0.5$ and 0.6 samples have vanished completely in the $y = 0.7$ sample (cf. Figs. 3a and b with c). The only reasonable interpretation of this observed XRD data is in terms of a subtle, but nonetheless quite reproducible, transition from single-phase pyrochlore to single-phase "defect fluorite" as a function of

composition y, with the co-existing two-phase region being centered around the $y = 0.6$ composition.

The $y = 0.6$ composition is thus in a two-phase region separating a Ti-rich pyrochlore solid solution field (for $y < \sim 0.54$) from a Zr-rich "defect fluorite" solid solution field ($\sim 0.68 < y < 1$). The disappearance of long range ordered $\mathbf{G} \pm \frac{1}{2}\langle 111\rangle^*$ satellite reflections on the "defect fluorite" side of the two-phase region, i.e., for the $y = 0.7$ and 0.8 samples, is again consistent with such an interpretation. The width of the miscibility gap around $y = 0.6$ appears to be in the range of ~0.54–0.68 for the sample annealed at 1350 °C for 20 days (see Fig. 2).

4.2. Electron diffraction

Electron diffraction investigation of the $y = 0.5$ and 0.7 solid-state synthesized samples confirmed the XRD results in that both samples were always found to be two-phase (consisting of an ordered pyrochlore and a 'disordered' defect fluorite) even after annealing at 1500 °C for 20 days. Fig. 4, for example, shows $\langle 130\rangle$ zone axis electron diffraction patterns (EDPs) typical of the (a) "defect fluorite" and (b) pyrochlore phases obtained from different grains in the nominally $y = 0.5$ solid-state sample. The indexation in Fig. 4 is with respect to the underlying fluorite type average structure in the case of the (a)"defect fluorite"-type EDP but with respect to a doubled pyrochlore unit cell in the case of the (b) pyrochlore phase EDP. The apparently split 'satellite' reflections centered around the $\mathbf{G} \pm \frac{1}{2}\langle 111\rangle^*$ regions of reciprocal space in the "defect fluorite"-type EDP are in fact part of a continuous 'smoke ring' like circle of diffuse intensity characteristic of many "defect fluorite" systems (see e.g., [8,15–18,21–22]). (The splitting of the 'satellite reflections' along the $\langle 312\rangle^*$ directions of reciprocal space in Fig. 4a is entirely consistent with such a 'smoke ring' like circle of diffuse intensity.) Note that the "defect fluorite" is further characterized by the absence of scattering at the

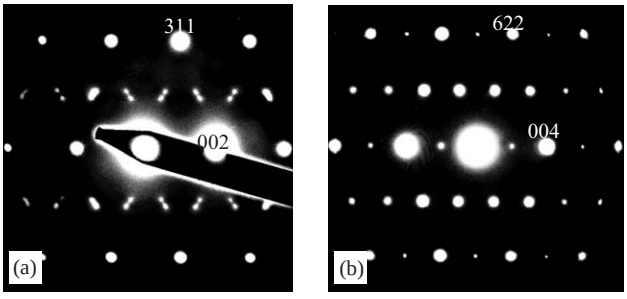

Fig. 4. Typical $\langle 130\rangle$ zone axis EDPs typical of the (a) "defect fluorite" and (b) pyrochlore phases obtained from different grains in the nominally $y = 0.5$ solid-state sample. The indexation is with respect to the underlying fluorite-type average structure in the case of: (a) but with respect to a doubled pyrochlore unit cell in the case of (b).

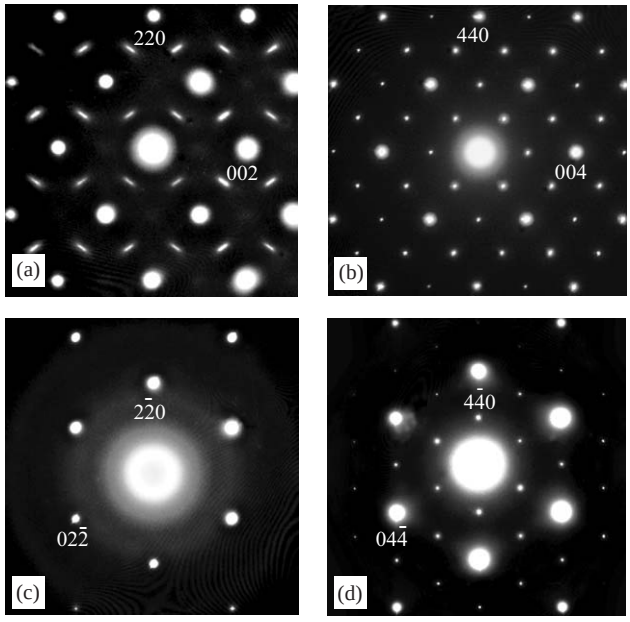

Fig. 5. Shows $\langle 110\rangle$ (a,b) and $\langle 111\rangle$ (c,d) zone axis EDPs typical of grains of the end-member "defect fluorite" (a,c) and pyrochlore (b,d) solid solution fields readily found in the two-phase $y = 0.6$ specimen. Indexation is again with respect to the underlying fluorite-type average structure in the case of (a) and (c) but with respect to a doubled pyrochlore unit cell in the cases of (b) and (d).

higher-order harmonic $\mathbf{G} \pm \langle 001\rangle^*$ regions of reciprocal space.

Electron diffraction of the MOD synthesized samples likewise confirmed the above XRD result that all compositions with $y < 0.6$ are indeed in a single phase pyrochlore-type solid solution while all compositions with $y > 0.6$ are in a single phase "defect fluorite"-type solid solution. The only composition at which both types of EDPs were simultaneously observed was the $y = 0.6$ composition. Typical $\langle 110\rangle$ (see Figs. 5a and b) and $\langle 111\rangle$ (see Figs. 5c and d) zone axis EDPs of the end-members of both these solid solution fields are shown in Fig. 5 and were readily and quite reproducibly found in the two-phase, $y = 0.6$ specimen. Given that sharp satellite reflections at the $\mathbf{G} \pm \frac{1}{2}\langle 111\rangle_p^*$ regions of reciprocal space only exist on the pyrochlore side of the two-phase region, the indexation in Fig. 5 is again with respect to the underlying fluorite-type average structure in the case of the "defect fluorite" phase EDPs in Figs. 5a and c but with respect to a doubled pyrochlore unit cell in the case of the pyrochlore phase EDPs shown in Figs. 5b and d.

Again note that the "defect fluorite" side of the two-phase region is characterized not by the total disappearance of scattered intensity at the $\mathbf{G} \pm \frac{1}{2}\langle 111\rangle_p^*$ regions of reciprocal space (and hence by the disappearance of metal ion and oxygen/vacancy ordering—see e.g., [8,15–18,21–22]) but rather by the smearing out of the $\mathbf{G} \pm \frac{1}{2}\langle 111\rangle_p^*$ type satellite reflections (see Fig. 5a) and the absence of scattering at the higher order

harmonic $\mathbf{G} \pm \langle 0\,0\,1\rangle_p^*$ regions of reciprocal space (see Fig. 5c). Such scattering (characteristic of the end-member "defect fluorite" solid solution field in this YZT system) is in fact strongly reminiscent of very similar scattering observed in the "defect fluorite" phase of the rare-earth sesquioxide stabilized cubic zirconias (see e.g., [8,15]). It is very strongly suggestive of a multi–$\mathbf{q}$ to single–$\mathbf{q} \sim \frac{1}{2}\langle 1\,1\,1\rangle_p^*$ mechanism [8,15] for the observed pyrochlore to "defect fluorite" phase transition in such systems.

4.3. Dielectric properties

Given the subtlety (see e.g., Figs. 3 and 5) of the composition-dependent "defect fluorite" to pyrochlore phase transition in this YZT system, we were intrigued to see whether or not the measured dielectric properties of the synthesized samples might show any evidence of a phase transition. Fig. 6 shows the measured dielectric properties of the MOD synthesized YZT samples annealed at 1350 °C for 5 days as a function of composition y at 1 V and 1 MHz frequency. No clear evidence for a two-phase region was apparent in the data, although the turning over of the dielectric loss curve as a function of y appears to be correlated with the transition. Why this should occur, however, is not clear to us.

The measured dielectric constant and dielectric loss of the $y = 0.1$ pyrochlore compound are 71 and 0.0028, respectively. (The previously reported dielectric constant for the end-member $Y_2Ti_2O_7$ pyrochlore composition [23] is very close to this i.e., 65 at room temperature [23].) Such a high dielectric constant and low dielectric loss suggests that the low y pyrochlore compounds have potential for use in microwave dielectric devices. In the low-frequency range, the dielectric loss of the $y = 0.1$ compound is essentially frequency independent. The dielectric constant, however, decreases quickly with increasing Zr content. It is measured to be only 11 for the $y = 0.8$ compound.

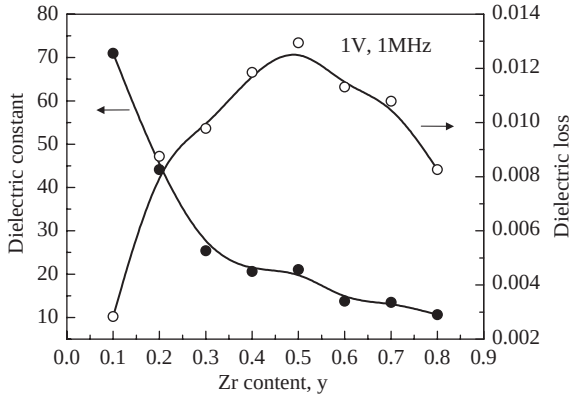

Fig. 6. Shows the measured dielectric constant and dielectric loss of the YZT samples annealed at 1350 °C for 5 days as a function of composition y at 1 V and 1 MHz frequency.

The dielectric loss, by contrast, increases rapidly upon initial substitution of Zr for Ti until it reaches an apparent maximum around $y = 0.5$ i.e., very close to the pyrochlore to "defect fluorite" phase transition (see Fig. 2). It subsequently reduces upon further increase in y. The same behavior was observed over the whole measured frequency range. It appears to also be correlated with the measured behavior of the oxide ion conductivity as a function of composition (cf. e.g., [2,5,9]).

5. Local crystal chemistry in the YZT system

The discovery that there is a genuine two-phase region separating a pyrochlore-type solid solution field ($0 \leqslant y \leqslant \sim 0.54$) from a "defect fluorite"-type solid solution field (from $\sim 0.68 \leqslant y \leqslant 1$) in this YZT system is significant and changes the way in which the results of the previous neutron diffraction investigation [2,9] should be interpreted. It means, for example, that disorder in the YZT pyrochlore-type solid solution field involves only the B_2O_6 (or $(Ti_{1-y}Zr_y)_2O(1)_{6-z}O(3)_z$) component sub-structure (see Fig. 1a) of the ideal pyrochlore structure type with the remaining OA_2 (or $O(2)Y_4$) component sub-structure (of anti-β cristobalite structure type—see Fig. 1b) remaining essentially inviolate right across the pyrochlore solid solution field. Why might/should this be so?

In order to attempt to obtain some crystal chemical insight into the refined behavior of this pyrochlore solid solution field [2,9], the dependence of the so-called valence least squares (VLS) functional [24]

$$\Delta = \sum\nolimits_i n_i [\Delta(\mathrm{AV})_i]^2 \quad (1)$$

upon the one unknown displacive variable of the ideal pyrochlore structure type, the x fractional co-ordinate of the O1 ion $= \frac{3}{8} + \varepsilon$, has been carefully investigated. (The previously reported crystallographic data [2,9], including composition, lattice parameters, occupancies etc. are simply taken as reported for the purposes of this exercise, despite some concerns that the actual compositions reported might be somewhat different given the results reported in the current paper.) In the above expression, note that the summation is over the 5 crystallographically independent sites (A, B, O1, O2 and O3) per pyrochlore unit cell, n_i represents the multiplicity of that site (appropriately weighted—see [9]) and $\Delta(\mathrm{AV})_i$ represents the deviation in calculated bond valence sum or apparent valence (AV) from the ideal valence for site i [25].

The ideal end member ($y = 0$) initial value of the functional Δ for the reported refined crystal structure of

Table 1
Bond valence sums, or apparent valences (AV_i's) [25], of the constituent ions of the $Y_2Ti_2O_7$ pyrochlore structure

Atom label	Multiplicity	$(AV)_i$ ($\varepsilon = 0.0458$)	$\Delta(AV)_i$ ($\varepsilon = 0.0458$)
Y^{3+}	16*c*	2.954	−0.046
Ti^{4+}	16*d*	4.106	+0.106
$O1^{2-}$	48*f*	1.934	−0.066
$O2^{2-}$	8*a*	2.516	+0.516

Fractional co-ordinates from [26]. $\Delta(AV)_i$ represents the deviation in apparent valence from the ideal valence for site *i*.

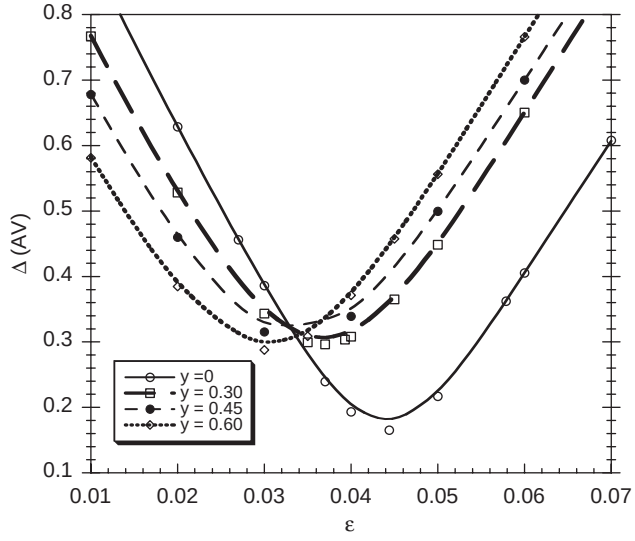

Fig. 7. Shows $\Delta(AV)$ as a function of Δ for each of the average pyrochlore structures reported by Heremans et al. [9] (i.e., $y = 0$, 0.30, 0.45 and 0.60).

$Y_2Ti_2O_7$ [26] is 2.550, of which 2.130 or 83.5% arises from the contribution of the over-bonded O2 ions. This is equivalent to an average mean square deviation in apparent valence $\Delta(AV) = \sqrt{(\sum_i n_i[\Delta(AV)_i]^2/\sum_i n_i)}$ of ~0.170. It is interesting to note that the O2 ion is significantly over-bonded (~25.8%) for this ideal end member ($y = 0$) pyrochlore structure [26] (see Table 1). The extent of this over-bonding could only be reduced by increasing the pyrochlore lattice parameter as does indeed occur for the necessarily disordered, non-zero y samples. It is also interesting to note that the AV's of the Y^{3+} and mixed $Zr_y{}^{4+}Ti_{1-y}{}^{4+}$ ions on the pyrochlore *A* and *B* sites vary much more rapidly with ε than the AV of the O1 ion (the AV of the O2 and O3 ions are independent of ε and only depend on the pyrochlore cell dimension). The minimum in $\Delta(AV)$ as a function of ε for a fixed pyrochlore cell dimension is thus essentially determined by the $\Delta(AV)$'s of the cation site positions. This explains why the pyrochlore cell dimension for $y = 0$ cannot simply expand to improve the AV of the O2 ion.

Table 2
Shows the predicted behavior of ε as a function of composition y (determined by minimization of $\Delta(AV)$) for each of the average pyrochlore structures reported by Heremans et al. [9] (i.e., $y = 0$, 0.30, 0.45 and 0.60)

Composition y	$\varepsilon_{predicted}$	$\varepsilon_{exptl.}$ (see [9])
0	0.0444	0.0458
0.30	0.0370	0.0423
0.45	0.0340	0.0360
0.60	0.0305	0.0272

The corresponding experimental values of ε reported by Heremans et al. [9] are also given.

Table 3
Shows AV's of the constituent ions of the refined $Y_2(Ti_{1-y}Zr_y)_2O_7$ structure type calculated for $y = 0.30$ at $\varepsilon = 0.037$. For this $y = 0.3$ compound, ~84.4% of the contribution to the functional Δ arises from the contribution of these Zr^{4+} and Ti^{4+} ions on the pyrochlore *B* site

Atom label	Multiplicity	(AV) ($\varepsilon = 0.037$)	$\Delta(AV)_i$ ($\varepsilon = 0.037$)
Y^{3+}	16*c*	3.058	+0.058
Ti^{4+}	16*d*	3.572	−0.428
Zr^{4+}	16*d*	4.939	+0.939
$O1^{2-}$	48*f*	1.938	−0.062
$O2^{2-}$	8*a*	2.379	+0.379
$O3^{2-}$	8*b*	1.552	−0.448

The behavior of $\Delta(AV)$ as a function of ε for each of the average pyrochlore structures reported by Heremans et al. [9] (i.e., $y = 0$, 0.30, 0.45 and 0.60) is shown in Fig. 7. In each case, a clear minimum was found at a value of ε which systematically reduced as a function of increasing y (see Table 2). The predicted decrease in ε as a function of y, however, is essentially linear whereas Heremans et al. [9] experimentally found more parabolic behavior. Note that the minimum value of $\Delta(AV)$ for the non-zero y compounds has increased significantly (relative to that for the end-member $y = 0$ compound) to a $\Delta(AV)$ of ~0.30 (see Fig. 7). The major reason for this increase is the simultaneous significant under-bonding of the Ti^{4+} ion and over-bonding of the Zr^{4+} ion on the average pyrochlore *B* site, as is clear from Table 3 which shows AV's calculated for $y = 0.30$ at $\varepsilon = 0.037$. For this $y = 0.3$ compound, ~84.4% of the contribution to the functional Δ arises from the contribution of these Zr^{4+} and Ti^{4+} ions on the pyrochlore *B* site (see Table 3).

The value of ε as well as the overall lattice parameter of the pyrochlore average structure clearly need to be carefully balanced as a function of y in such a way as to minimize this unavoidable large amplitude contribution. We believe this is the principal crystal chemical reason underlying the refined decrease of ε as well as the increasing pyrochlore unit cell dimension with

increasing y (according to [2,9], $a_{pyr} \sim 10.09$ Å and $\varepsilon \sim 0.421-0.375 = 0.046$ at $y = 0$ while $a_{pyr} \sim 10.24$ Å and $\varepsilon \sim 0.411-0.375 = 0.036$ at $y = 0.45$). Table 3, however, also shows that the partially occupied O3 site is substantially under-bonded for this $y = 0.3$ compound while the over-bonding of the fully occupied O2 site has reduced.

In addition to these enthalpic bond valence sum-type considerations, there is one further potentially quite important energetic term that needs to be taken into account when attempting to understand the crystal chemistry of the non-zero y compounds. This is the effect of non-bonded O–O interactions [27]. The initially unoccupied O3 site in the ideal pyrochlore structure type (see Fig. 1a) is octahedrally co-ordinated by six nearest neighbour O1 oxygen ions at a non-bonded O1–O3 oxygen–oxygen separation distance d_{O-O} given by $d_{O-O} = (\frac{1}{4} - \varepsilon)a_{pyr}$. At $y = 0$, $a_{pyr} \sim 10.09$ Å while $\varepsilon \sim 0.421-0.375 = 0.046$ i.e., $d_{O-O} = 2.06$ Å [2,9]. Non-bonded O–O distances as unrealistically short as these are known to be energetically very costly [27] and imply the existence of considerable local strain distortion associated with the simultaneous occupancy of neighboring O1 and O3 sites as well the necessity for very significant local displacive relaxation, principally local repulsion or static displacement of the O1 ions away from the neighboring occupied O3 sites with a magnitude ($\sim 0.4-0.5$ Å for $y \sim 0$) dependent upon the value of y. According to [2,9], for example, $a_{pyr} \sim 10.24$ Å while $\varepsilon \sim 0.411-0.375 = 0.036$ at $y = 0.45$ i.e., $d_{O-O} = 2.19$ Å at $y = 0.45$. This would imply a local static displacement of an O1 ion away from any neighboring occupied O3 site with a magnitude ~0.3–0.4 Å. (While the magnitude of this local shift could be expected to reduce as y increases, the rapidly increasing occupancy of the O3 site itself as y increases leads to a sharp increase of the refined average value of the β_{11} anisotropic displacement parameter of this O1 ion ("... indicating an increased thermal vibration amplitude ... toward the initially vacant 8b (or O(3)) site ..." [2,9]).

Non-long-range ordered localized distortions of this type, including local expansion and contraction of the size of the $BO(1)_6$ octahedra (see Fig. 1a) depending upon whether or not the B site is locally occupied by a Zr^{4+} or a Ti^{4+} ion, can be expected to give rise to considerable local strain and therefore induce correlations from one such average pyrochlore unit cell to the next thereby giving rise to the structured diffuse scattering apparent in appropriately exposed EDPs of the non-zero y samples (see, for example, the close to $\langle 111 \rangle$ zone axis EDP of the $y = 0.50$ specimen shown in Fig. 8). As has long been recognized [28] the detection and successful modeling of such complex structured diffuse scattering is the key to fully understanding the nature of disorder in such systems.

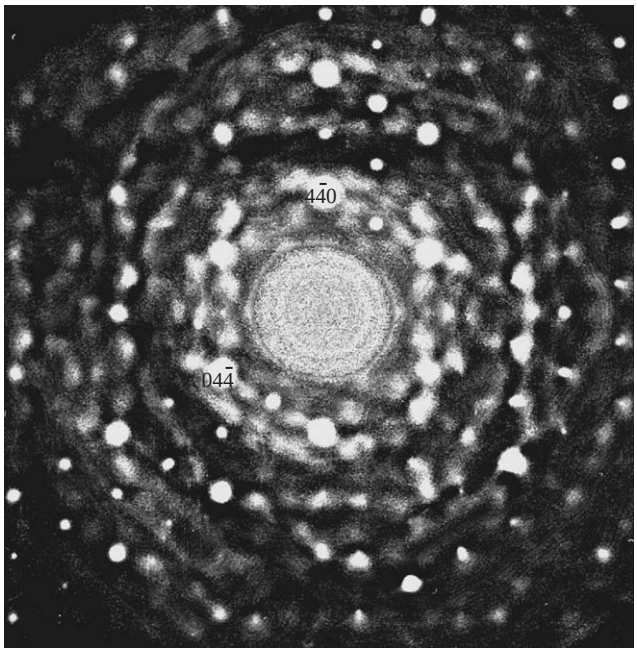

Fig. 8. Close to $\langle 111 \rangle$ zone axis EDP of a $y = 0.50$ pyrochlore specimen showing structured diffuse scattering indicative of local short-range order and associated structural relaxation.

Why then is there experimentally a phase transition from a pyrochlore to a "defect fluorite" solid solution at $y \sim 0.54$? One possible reason is the $N(1-N)$ effect i.e., around $y \sim 0.5$, the disordered B and O3 sites each become ~one-half occupied (according to [2,9], the average occupancy of the O3 site at $y = 0.60$ is ~0.5). This means that there is less and less local flexibility to accommodate the local distortions and shifts required by the above crystal chemical considerations as y increases until (at $y \sim 0.54$) the strain energy associated with mixed occupancy of the pyrochlore B site and the non-bonded O1–O3 interactions presumably become too difficult to accommodate within an average pyrochlore structure type and a phase transition to a "defect fluorite" structure type takes place.

References

[1] H.L. Tuller, P.K. Moon, Mater. Sci. Eng. B 1 (1988) 171–191.
[2] B.J. Wuensch, K.W. Eberman, C. Heremans, E.M. Ku, P. Onnerud, E.M.E. Yeo, S.M. Haile, J.K. Stalick, J.D. Jorgensen, Solid State Ionics 129 (2000) 111–133.
[3] K.R. Kendall, C. Navas, J.K. Thomas, H.-C. zur Loye, Solid State Ionics 82 (1995) 215–223.
[4] S. Kramer, M. Spears, H.L. Tuller, Solid State Ionics 72 (1994) 59–66.
[5] P.K. Moon, H.L. Tuller, Mater. Res. Soc. Symp. Proc. 135 (1989) 149–163.
[6] T.-H. Yu, H.L. Tuller, Ceram. Trans. 65 (1996) 3–11.
[7] M.A. Subramanian, G. Aravamudan, G.V. Subba Rao, Prog. Solid State Chem. 15 (1983) 55–143.
[8] R.L. Withers, J.G. Thompson, P.J. Barlow, J.C. Barry, Aust. J. Chem. 45 (1992) 1375–1395.

[9] C. Heremans, B.J. Wuensch, J. Solid State Chem. 117 (1995) 108–121.
[10] M. Glerup, O.F. Nielsen, F.W. Poulsent, J. Solid State Chem. 160 (2001) 25–32.
[11] N. Kim, C.P. Grey, J. Solid State Chem. 175 (2003) 110–115.
[12] J. Chen, J. Lian, L.M. Wang, R.C. Ewing, Phys. Rev. Lett. 88 (2002) 105901–105904.
[13] A. Kaiser, A.J. Feighery, D.P. Fagg, J.T.S. Irvine, Ionics 4 (1998) 215–219.
[14] A.J. Feighery, J.T.S. Irvine, D.P. Fagg, A. Kaiser, J. Solid State Chem. 143 (2003) 273–276.
[15] Y. Tabira, R.L. Withers, J.C. Barry, L. Elcoro, J. Solid State Chem. 159 (2001) 121–129.
[16] S. Suzuki, M. Tanaka, M. Ishigame, J. Phys. C 20 (1987) 2963–2972.
[17] S. García-Martín, M.A. Alario-Franco, D.P. Fagg, A.J. Feighery, J.T.S. Irvine, Chem. Mater. 12 (2000) 1729–1737.
[18] T.R. Welberry, R.L. Withers, S.C. Mayo, J. Solid State Chem. 115 (1995) 43–54.
[19] B. Noläng, Inst. Materialkemi, Ångströmlaboratoriet, Box 538, SE-751 21, Uppsala, Sweden.
[20] C.J. Brinker, G.W. Scherer, Sol–Gel Science—The Physics and Chemistry of Sol–Gel Processing, Academic Press, New York, 1990, pp. 29–30.
[21] J.G. Allpress, H.J. Rossell, J. Solid State Chem. 15 (1975) 68–78.
[22] R. Miida, M. Tanaka, H. Arashi, M. Ishigame, J. Appl. Cryst. 27 (1994) 67–73.
[23] F. Jona, G. Shirane, R. Pepinsky, Phys. Rev. 98 (1955) 903–909.
[24] V.S. Urusov, I.P. Orlov, Crystallogr. Rep. 44 (1999) 736–760.
[25] N.E. Brese, M. O'Keeffe, Acta Crystallogr. B 47 (1991) 192–198.
[26] S.M. Haile, B.J. Wuensch, E. Prince, Mater. Res. Soc. Symp. Proc. 166 (1990) 81–86.
[27] B.B. Hyde, Z. für Kristallogr. 179 (1987) 205–213.
[28] H.J. Rossell, H.G. Scott, J. Phys. Colloque C7 38 (1977) C7–C28.